Long-range entanglement in quantum dots with Fermi-Hubbard physics

Sanaa Abaach [1,*] Mustapha Faqir [2,†] and Morad El Baz [1,‡]

[1]*ESMaR, Faculty of Sciences, Mohammed V University, BP 8007 Rabat, Morocco*

[2]*LERMA Laboratory, Aerospace Engineering School, Université Internationale de Rabat, 11100 Sala al Jadida, Morocco*

(Received 26 April 2022; accepted 2 August 2022; published 22 August 2022)

The range of entanglement in quantum dots, under the effect of the Coulomb interaction and the system's size, is investigated. As ququart systems, naturally described by the Fermi-Hubbard model, we show that quantum dots supply long-range entanglement up to the third neighbor. In conjunction with that and using the lower bound of concurrence, we show that the Coulomb interaction can be adjusted to create and increase entanglement between distant parties as well. A rigorous description of the pairs is given in terms of a local half-filled state associated with each pair with an electron number $N = 2$ and a spin $S = 0$. A thorough study of this state provides a proper explanation related to the pairwise entanglement, namely, its amount and its behavior under the effect of the Coulomb interaction together with the system's size. In addition, we show that the confinement state of quantum dots is genuinely four-partite entangled with a maximum amount for the smallest size $L = 4$.

DOI: 10.1103/PhysRevA.106.022421

I. INTRODUCTION

As a swiftly expanding and cross-disciplinary topic, quantum entanglement has been a subject of various studies that have attracted many leading theorists and experimentalists from physics, computer science, and electronic engineering in recent years. Mostly due to its nonlocal [1] connotation, this primarily intriguing feature of quantum mechanics is regarded as a precious resource and a key ingredient in many striking achievements that have been witnessed in the past decade in quantum communication and information processing [2–4].

Over the past several years, there has been a heightened interest in quantum many-body systems in favor of quantum information and vice versa [5]. This interest has been triggered as a consequence of the imperative need to enhance the understanding of the physics of many-body systems for the purpose of operating the basic unit of quantum information, i.e., the qubit, as well as for building scalable devices designed to implement quantum information tasks in a very accurate and controlled way. Among the most scalable and time-coherent platforms, dedicated to implement quantum information schemes, are quantum dot (QD) systems [6–8]. Quantum dots are semiconductor nanocrystals, often referred to as artificial atoms, where the carriers' motion is quantized in all the spatial directions giving rise to discrete energy levels (quantum confinement effect). Semiconductor QDs are naturally described by the Fermi-Hubbard (FH) model in the low-temperature and strong-Coulomb-interaction regime [9]. This property provides a simplified framework for the understanding of the behavior of QDs. As a matter of fact, the FH model is a simple approach that describes interacting spin-$\frac{1}{2}$ fermions in many-body systems. The Coulomb repulsion interaction governing the fermions in this approach is one of the physical effects that dominates the electronic properties of QD systems [10]. Hence, a better understanding of the Hubbard physics allows an accurate experimental tunability of the electron numbers in each quantum dot, as well as other parameters, using gate voltages [9].

The ground state of the FH model is considered as a natural source of entanglement. Moreover, a closer look at the nature of entanglement in the FH models ground state may reveal itself powerful to enhance the information transfer in quantum communications. Indeed, the quantum states of such a model are ququart states ($d = 4$), giving rise to an enlarged Hilbert space. This could provide a larger information capacity and an increased noise resilience [11] which could strongly promote the use of this model to carry out quantum information tasks. Nonetheless, increasing the dimension paves the way to the well-known issue of entanglement quantification for mixed states in higher-dimensional systems. In view of this fact, many questions are still open in the FH model and little is known about the details of entanglement, such as the behavior of pairwise entanglement as well as the range of entanglement in the weak-interaction regime. In this regard, a particular lower bound of concurrence (LBC) has been recently suggested [12], providing a good estimation of mixed states' bipartite entanglement in higher dimensions. Using this measure, we will show, for instance, that in the weak-interaction regime, the pairwise entanglement increases with the growth of the Coulomb interaction in contrast to the local entanglement [13,14].

In general, the most natural way of creating a large amount of entanglement between two or more parties, in low-dimensional systems, requires the presence of strong correlations. In most qubit systems with short-range interactions and with periodic boundary conditions, the entanglement between a pair of particles declines rapidly with distance and could vanish even for distances larger than two sites such as the case of the Ising model with a transverse field [15]. It can

*sanaa_abaach@um5.ac.ma
†mustapha.faqir@uir.ac.ma
‡morad.elbaz@um5.ac.ma

also be restricted only to nearest neighbors in the Heisenberg model [16]. From the point of view of quantum information, an even more appealing goal would be the ability to create a large amount of entanglement between distant and generally not directly interacting constituents. This can be conveniently exploited for an efficient implementation of spin-chain-based quantum information schemes [17,18]. Moreover, it has been shown that the ground state of some spin chains with open boundary conditions and finite correlation length can supply large values of end-to-end entanglement between the end sites of the chain [19]. In the present paper a characteristic case of an open array with size $L = 4$ will provide an important end-to-end entanglement where the range of entanglement extends to the third neighbor, while for $L > 4$ the range can be created and extended to the second and third neighbors under the effect of the Coulomb interaction.

In this study we focus on finite-size systems as appropriate systems for numerical treatment that can be extrapolated to larger-size lattices. Furthermore, they are easily controlled and manipulated experimentally in nanotechnological applications. A pivotal analysis of our results will be presented in terms of a local half-filled state (LHFS) describing each pair with two electrons. A complete knowledge about the LHFS and its associated probability will provide primary details regarding the amount of entanglement and its behavior under the effect of the Coulomb interaction as well as the system's size. The principal cornerstones of our work are presented in Sec. II: The one-dimensional FH model, which provides an adequate approach for the description of QD systems, and the LBC as a measure of pairwise entanglement. The aforementioned measure allows us in Sec. III to reveal the range of entanglement as well as the behavior of pairwise entanglement, which proves to be distinct from that of the well-known local entanglement. Focusing on the smallest size that we simulated, $L = 4$, a detailed explanation of the pairwise entanglement properties is presented in Sec. IV, showing the presence of two competing effects responsible for the increase in pairwise entanglement: The mixing effect and the inherent effect associated with the LHFS. A summary, conclusions, and perspectives for future work are presented in Sec. V.

II. MODEL AND FORMALISM

A. Fermi-Hubbard model

An array of QDs can be modeled by the one-dimensional FH approach [9,20]. Assuming that the hopping is bounded by the nearest-neighbor lattice sites, the simplest expression of the Hamiltonian corresponding to the model [21] is formulated as

$$H = -t \sum_{i,\sigma} (c^{\dagger}_{i,\sigma} c_{i+1,\sigma} + c^{\dagger}_{i+1,\sigma} c_{i,\sigma}) + u \sum_{i} n_{i,\uparrow} n_{i,\downarrow}, \quad (1)$$

where $c^{\dagger}_{i,\sigma}$ and $c_{i,\sigma}$ are the creation and annihilation fermionic operators, respectively, attached to site i with spin $\sigma = \{\uparrow, \downarrow\}$ (indicating spin-up or spin-down electron), and $n_{i\sigma} = c^{\dagger}_{i,\sigma} c_{i,\sigma}$ is the corresponding number operator. In addition, t is the hopping amplitude, associated with the tunneling of electrons between the neighboring sites, whereas u is the on-site electron-electron Coulomb interaction. To describe the QDs, a simple approximation is to regard each dot as having one valence orbital (s orbital) with a single energy level; accordingly, each QD is able to hold up to two electrons with opposite spins in compliance with the Pauli exclusion principle. Thereby electrons have four possibilities in occupying a single site: $|0\rangle$, $|\uparrow\rangle$, $|\downarrow\rangle$, and $|\uparrow\downarrow\rangle$ (standing for no electron, one electron having a spin up, one electron having a spin down, and two electrons, respectively).

When the repulsion interaction u within the sites is too strong compared to the hopping amplitude t, the tunneling of electrons is blocked, leading to a clear observation of the quantum confinement effect in the FH model. This is analogous to the creation of potential barriers between the sites, which prevent electrons from moving outside. Experimentally, such barriers can be produced by modulating the potentials using gate electrodes in order to control the tunneling of electrons between quantum dots [9]. Indeed, from an experimental point of view, one of the commonly studied and experimentally employed quantum dot devices are GaAs/AlGaAs semiconductor heterostructures that grow by molecular-beam epitaxy. Into the interface between GaAs and AlGaAs, free electrons are strongly confined in one direction, which thus induces a two-dimensional electron gas (2DEG). By locally depleting the 2DEG, using metal gate electrodes on the surface of the heterostructure, the electrons can now be well confined in the remaining two dimensions. The control of FermiHubbard parameters is reached by adjusting the potential landscape in the 2DEG through gate electrodes. These gates include plunger gates and barrier gates that are designed to tune the single-particle energy offsets, the chemical potential of individual dots, the tunnel couplings (t) between two dots as well as the on-site (u) and the intersite Coulomb interaction energies.

In typical structures [9,20,22], u is of the order of a few meV and t is tunable by gate voltages from $t \sim 0$ to $t \sim 100\ \mu$eV. In addition, quantum dot systems can be cooled down to a few tens of mK, which ensures the thermal energy to be significantly lower than the other energy scales of the system ($k_T \ll t \ll u$). In the following we will consider the dimensionless quantity $U = u/t$ as the main parameter in the model.

B. Lower bound of concurrence

The absence of a proper measure of entanglement for systems beyond the 2×2 and 2×3 dimensions forces us to settle for a measure of the lower bound of entanglement instead of analytical exact results. Some operational lower bounds of the concurrence for any dimensional mixed bipartite quantum states have been presented by using positive partial transposition and realignment separability criteria [23,24], which can detect some bound entangled states but not all. These bounds are exact for some special classes of states. In [25] another lower bound on the entanglement of formation for bipartite states was presented from a separability criterion [26] based on a nondecomposable positive map which operates on state spaces with even dimension, $N \geqslant 4$, leading to a class of nondecomposable optimal entanglement witnesses. In [27] a derived lower bound of concurrence based

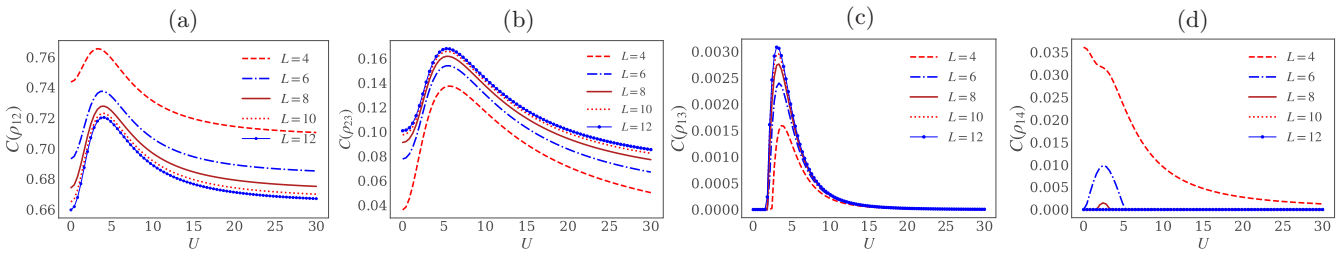

FIG. 1. Lower bound of concurrence (2), associated with the pairs (a) ρ_{12}, (b) ρ_{23}, (c) ρ_{13}, and (d) ρ_{14}, as a function of U for various system sizes up to $L = 12$.

on the local uncertainty relation criterion complements and improves the results shown in [24].

In [12] the authors derived an analytical lower bound of concurrence for arbitrary bipartite quantum states by decomposing the joint Hilbert space into many $(2 \otimes 2)$-dimensional subspaces, which does not involve any optimization procedure and gives an effective evaluation of entanglement. This lower bound was recently extended to an arbitrary N-partite state [28,29] which detects quantum entanglement of some states better than some separability criteria. For an arbitrary bipartite system of dimension $d \times d$, the concurrence $C(\rho_{ij})$ [12] satisfies

$$\tau_2(\rho_{ij}) = \frac{d}{2(d-1)} \sum_{\alpha}^{d(d-1)/2} \sum_{\beta}^{d(d-1)/2} C_{\alpha\beta}^2 \leqslant C^2(\rho_{ij}), \qquad (2)$$

where

$$C_{\alpha\beta} = \max\left\{0, \lambda_{\alpha\beta}^{(1)} - \lambda_{\alpha\beta}^{(2)} - \lambda_{\alpha\beta}^{(3)} - \lambda_{\alpha\beta}^{(4)}\right\}. \qquad (3)$$

In our case, ρ_{ij} is the pairwise density matrix of a four-level system (i.e., ququarts); for concreteness we take $i < j$. Here $\lambda_{\alpha\beta}^{(m)}$ are the square roots of the nonzero eigenvalues of the non-Hermitian matrix $\rho_{ij}\tilde{\rho}_{(ij)\alpha\beta}$ such that $\lambda_{\alpha\beta}^{(m)} > \lambda_{\alpha\beta}^{(m+1)}$ for $m = 1$, 2, 3, or 4 and

$$\tilde{\rho}_{(ij)\alpha\beta} = (G_\alpha \otimes G_\beta)\rho_{ij}^*(G_\alpha \otimes G_\beta). \qquad (4)$$

Here G_α is the αth element of the group SO(d) spanned by $\frac{d(d-1)}{2}$ generators and G_β is defined similarly since the two subsystems have the same dimension d.

The left-hand side of the inequality in (2) can be effectively computed, providing thus a solid lower bound of concurrence and entanglement. Although being deficient in granting all the details about the amount of entanglement, this LBC imparts precious information that is not obtainable otherwise. The efficiency of the LBC is manifested in the fact that it can detect mixed entangled states with a positive partial transpose [28] and that for fully separable multipartite state it is equal to zero.

III. RANGE OF ENTANGLEMENT AND SIZE EFFECT

In this section we analyze the pairwise entanglement behavior, under the effect of the Coulomb interaction U in a finite-size array of QDs, formally described by the FH model. Furthermore, the range of entanglement under the system's size effect is investigated. This will establish the peculiarities of this type of entanglement compared to the single-site entanglement. Figure 1 gives us some insight in this regard. An initial increase of U in the weak-coupling regime could give rise to an appreciable growth in the pairwise entanglement, in contrast to the local entanglement that decays instantly with U [13,14]. Since entanglement is a crucial ingredient for quantum information tasks, any improvement or increase in this resource will make a prominent contribution in quantum information. In this regard, U proves its potency in increasing and, more importantly, creating entanglement within the pairs and this will play a significant role in the direction that employs spin chains as quantum channels [30]. The calculations were done by exact diagonalization of the Fermi-Hubbard model [31,32].

A. Pairwise entanglement and size effect

In terms of the system's size, Fig. 1 shows that as the system grows in size, the pairwise entanglement $C(\rho_{ij})$ decays for all the pairs ρ_{ij} $(i < j)$ with j even but increases instead for all the pairs where j is odd. Generally, this can be interpreted by the fact that the pairs at the borders ρ_{12} and $\rho_{L-1,L}$, with $\rho_{12} = \rho_{L-1,L}$ by mirror reflection symmetry, are less correlated with the remaining sites according to the monogamy of entanglement as they have to conserve the higher amount of entanglement. This is especially shown for the smallest size $L = 4$, where in this case $C(\rho_{12})$ is the highest quantity, as shown in Fig. 1(a). However, with the increase of the size, the influence of the other sites becomes increasingly important; consequently, the pairwise entanglement $C(\rho_{12})$ and $C(\rho_{L-1,L})$ at the borders, with j even, decays with the system's size.

Since the pairs at the borders have an even j, their nearest pairs, i.e., ρ_{23} and $\rho_{L-2,L-1}$ (with $\rho_{23} = \rho_{L-2,L-1}$ due to the mirror reflection symmetry), necessarily have an odd index j. Considering, for instance, the fact that $C(\rho_{12})$ decays as L grows, the monogamy of entanglement in this case forces the quantum correlations, on one hand between sites 1 and 3 and on the other hand between 2 and 3, to be increased instead and this is the reason why the pairwise entanglement $C(\rho_{13})$ and $C(\rho_{23})$, in Fig. 1, grows with L. The same reasoning, based on the monogamy of entanglement, explains the increase of the pairwise entanglement $C(\rho_{ij})$ with j even and the decrease of $C(\rho_{ij})$ for j odd, with the increase of the size L of the system.

B. Range of entanglement

From the point of view of the distance effect, since intuitively the presence of direct and strong correlations provide great amounts of entanglement, the adjacent sites [Figs. 1(a) and 1(b)], for instance, should reveal a larger amount of

entanglement compared to the distant sites [Figs. 1(c) and 1(d)] at $U = 0$. Indeed, the previous behavior is in agreement with the monogamy of entanglement which broadly stipulates that if two systems are strongly entangled with each other, then each of them cannot be entangled very much with other systems. In addition to that, when increasing U while staying in the weak-coupling regime, the entanglement (LBC) grows considerably for the adjacent sites but insubstantially for the distant sites (except for ρ_{14} when $L = 4$). After reaching a maximal value, the LBC diminishes asymptotically to a nonzero value for nearest-neighbor sites and to zero for distant sites.

One of the most important aspects characterizing spin chain systems is their ability to distribute entanglement between distant parties. In this regard it is clearly shown in Fig. 1(d) that at $U = 0$, the range of entanglement extends to the third-neighbor site for the smallest size system $L = 4$, while for $4 < L < 10$ the range of entanglement is restricted to the nearest-neighbor sites. Nevertheless, it is created and extended again to the third-neighbor site with an optimal choice of U in a specific interval, whereas with the size growth $L \geqslant 10$ the range of entanglement is restricted to the second neighbors again in a specific interval of U (Fig. 1). Beyond that the pairwise entanglement vanishes for distances larger than single neighboring site when U takes large values.

Finding an appropriate interpretation for the increase in pairwise entanglement as a function of U in the weak-coupling regime can seem to be rather complicated as the question concerns the larger sizes. To circumvent this initially, in the next section our study will be based on the smallest size system $L = 4$, where a detailed explanation of the aforementioned pairwise entanglement behavior can be easily analyzed and afterward generalized to larger system sizes.

IV. ENTANGLEMENT AND LOCAL HALF-FILLED STATE

A. Local entanglement

For a chain with open boundary conditions, due to a lack of translational invariance, the local entanglement (referring to the entanglement of a given site with the rest of the chain) is not expected to be the same for each site i. However, the mirror reflection symmetry translates into the constraint $E(\rho_i) = E(\rho_{L-i+1})$, where $E(\rho) = -\mathrm{Tr}(\rho \log_2 \rho)$ is the von Neumann entropy and

$$\rho_i = v_i|0\rangle\langle 0| + s_{i\uparrow}|\uparrow\rangle\langle\uparrow| + s_{i\downarrow}|\downarrow\rangle\langle\downarrow| + d_i|\uparrow\downarrow\rangle\langle\uparrow\downarrow|, \quad (5)$$

with

$$d_i = \mathrm{Tr}(n_{i\uparrow}n_{i\downarrow}\rho_i) = \langle n_{i\uparrow}n_{i\downarrow}\rangle, \quad s_{i\uparrow} = \langle n_{i\uparrow}\rangle - d_i,$$
$$s_{i\downarrow} = \langle n_{i\downarrow}\rangle - d_i, \quad v_i = 1 - d_i + s_{i\uparrow} + s_{i\downarrow}. \quad (6)$$

For the FH model at half filling, $\langle n_{i\uparrow}\rangle = \langle n_{i\downarrow}\rangle = \frac{1}{2}$ and $s_{i\uparrow} = s_{i\downarrow} = s_i = \frac{1}{2} - d_i$. Consequently, the corresponding von Neumann entropy is

$$E(\rho_i) = -2d_i \log_2 d_i - 2\left(\tfrac{1}{2} - d_i\right)\log_2\left(\tfrac{1}{2} - d_i\right). \quad (7)$$

It can be seen from Fig. 2 for $L = 4$ [Fig. 2(a)] and $L = 12$ [Fig. 2(b)] that while behaving similarly under the effect of U, the amount of local entanglement at the end sites, $E(\rho_1) = E(\rho_L)$, is less than that in the inner sites, $E(\rho_i)$ with $1 < i < L$. It is quite clear that at $U = 0$ the electrons can move freely in the array in such a way that each site has the same probability of being singly occupied s_i, doubly occupied d_i, or empty v_i. Focusing on the smallest size $L = 4$, this is confirmed from the inset in Fig. 2(b), where at $U = 0$, $s_i = d_i = \frac{1}{4}$, thus explaining why the $E(\rho_i)$ at the ends and the inner sites have the same value. With increasing U the local entanglement at the ends exhibits a faster decrease compared to the entanglement in the middle of the chain $E(\rho_1) = E(\rho_4) < E(\rho_2) = E(\rho_3)$. This can be easily explained following the same reasoning mentioned previously by noticing in the inset in Fig. 2(a) that as the repulsion interaction increases the sites at the ends favor the single occupancy ($s_\uparrow$ or $s_\downarrow$) more than the sites in the middle and therefore the correlations created at the end sites tend to degrade faster with the increase of U. The same behavior is consistently applied to large sizes. Nevertheless, the sites in the middle retain the same amount of entanglement, as shown in Fig. 2(b), considering the fact that the effect of the borders becomes negligible as we move away from the ends. Consequently, the occupation probabilities s_i and d_i in this case becomes equal for all the middle sites, thus resulting in equal amounts of entanglement.

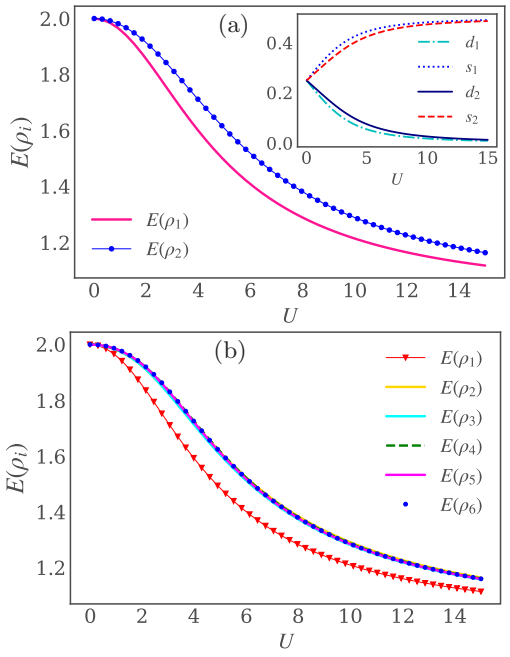

FIG. 2. Local entanglement (a) $E(\rho_1) = E(\rho_L)$ and $E(\rho_i)$ with $1 < i < L$ [Eq. (7)] at the ends and the middle of the chain, respectively, as a function of U for system size (a) $L = 4$ and (b) $L = 12$. The inset in (a) shows the effect of U on the single- and double-occupation probabilities s_i and d_i, respectively, at the end sites ($i = 1, 4$) and the middle sites ($i = 2, 3$).

It is worth mentioning that, even though the on-site interaction U is assumed to be the same at all the sites, the situation becomes equivalent to a chain with $U_e > U_m$ [33] for finite U, where U_e and U_m denote the end and the middle on-site Coulomb interactions, respectively. Generally, the inequality $U_e > U_m$ expresses the fact that the occupation probabilities associated with the four configurations are not equal for all the sites. Notably, the occurrence of double occupancy at the end sites is more disfavored in comparison to that at the middle

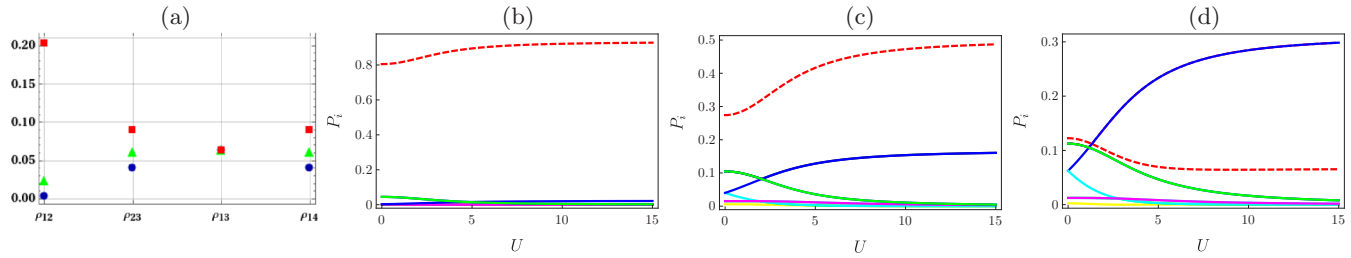

FIG. 3. (a) Probabilities corresponding to the 16 basis states for each pair at $U = 0$ with $L = 4$. The basis states with $N = 2$ and $S = 0$ are marked by red squares, those with $N = \{1, 3\}$ and $S = \pm\frac{1}{2}$ by green triangles, and those with $N = \{0, 4\}$ and $S = 0$ and with $N = 2$ and $S = \pm 1$ by blue circles. Also shown are the probabilities P_k associated with the 4^2 eigenstates $|\psi_k\rangle$ of (b) ρ_{12}, (c) $\rho_{23} = \rho_{14}$, and (d) ρ_{13}. The P_{LHFS} associated with the LHFS is marked by a red dashed line.

sites. This scenario is different for periodic chains where the local entanglement for all the sites is the same [13,14].

At $U \to \infty$ the tunneling of electrons is blocked, yielding thus the confinement state, where each site confines one electron with spin up or spin down. At this stage the probability of the different occupation configurations becomes equal at each site. As a result, the entanglement at each site becomes the same in the confinement state. Understanding the behavior of the local entanglement behavior will partly explain the behavior of the pairwise entanglement discussed hereafter.

B. Pairwise entanglement at $U = 0$

For the purpose of analyzing the pairwise entanglement behavior, we have to discuss generally the state characterizing the pairs at $U = 0$ and without loss of generality we consider $L = 4$. In this case, the half-filled single band array is defined by a fixed total number of electrons, 4, and a null total spin. However, the situation is different for the local pairs where a given (odd or even) number of electrons $N = \{0, 1, 2, 3, 4\}$ can be associated with each pair with a specific total spin $S = \{-1, -\frac{1}{2}, 0, \frac{1}{2}, 1\}$. Henceforth, the state describing each pair is represented by a mixture

$$\rho_{ij} = \sum_k P_k |\psi_k\rangle\langle\psi_k|, \tag{8}$$

where $\{|\psi_k\rangle\}$ are the possible states corresponding to a given number N and a total spin S defined above.

As previously outlined, at $U = 0$ each site has the same probability $\frac{1}{4}$ to be in one of the four possible states $|\uparrow\rangle$, $|\downarrow\rangle$, $|\uparrow\downarrow\rangle$, or the vacuum state $|0\rangle$. Nevertheless, the different pairs are described differently and they exhibit dissimilarity in the occupation probabilities associated with the 16 (4^2) basis states of each pair. Note from Fig. 3(a) that the pairs of neighboring sites located at the ends of the array, $\rho_{12} = \rho_{34}$, have a relatively high probability to be in the states $|\uparrow, \downarrow\rangle$, $|\downarrow, \uparrow\rangle$, $|\uparrow\downarrow, 0\rangle$, and $|0, \uparrow\downarrow\rangle$, i.e., states with $N = 2$ and $S = 0$, compared to other states. The other pairs exhibit a different behavior and as such it becomes obvious that the pairwise entanglement cannot be the same between all pairs at $U = 0$, contrary to the local entanglement.

It is worth mentioning that all the states $|\psi_k\rangle$ in the decomposition (8) are degenerate due to particle number conservation and spin symmetry, except the state with $N = 2$ and $S = 0$, which is given by $(\alpha|\uparrow, \downarrow\rangle + \beta|\downarrow, \uparrow\rangle + \gamma|\uparrow\downarrow, 0\rangle + \delta|0, \uparrow\downarrow\rangle)$, hereafter referred to as the local half-filled state. Furthermore, for all the pairs at $U = 0$, it is the state that possesses the highest probability in contrast to the others, as reflected in Fig. 3. Given the fact that the LHFS is the dominant state as well as a highly entangled state (maximally entangled for $|\alpha| = |\beta| = |\gamma| = |\delta| = \frac{1}{2}$ at $U = 0$) in the mixture (8), the behavior of the pairwise entanglement will be essentially dominated by the LHFS entanglement behavior itself. Henceforth, in the following the pairwise entanglement behavior will be explained based on the LHFS.

In Fig. 3(b) it is shown that the pair ρ_{12} has a very high probability, which exceeds 0.8, to be in the LHFS. This is expected because, as we have pointed out, the states $|\uparrow, \downarrow\rangle$, $|\downarrow, \uparrow\rangle$, $|\uparrow\downarrow, 0\rangle$, and $|0, \uparrow\downarrow\rangle$ are the most favored states for the pair ρ_{12} [Fig. 3(a)], followed by the pair ρ_{23} and ρ_{14} and finally ρ_{13}. As the mixture is generally dominated by the LHFS, it is evident that the higher the probability of being in this state, the higher the pairwise entanglement will be. This is what explains the pairwise entanglement at $U = 0$ observed in Fig. 1, where, considering $L = 4$ for illustrative purposes, the highest amount of entanglement goes to the pair ρ_{12} followed by ρ_{23}, ρ_{14}, and finally ρ_{13}. The same reasoning applies for $L > 4$, where the amount of pairwise entanglement $C(\rho_{ij})$ depends primarily on the quantity P_{LHFS} (the probability of a pair being in the LHFS) in such a manner that, for a fixed L, the higher P_{LHFS} is, the higher the pairwise entanglement $C(\rho_{ij})$ is and vice versa.

Returning to the size effect on pairwise entanglement $C(\rho_{ij})$ for an even or odd index j, discussed in Sec. III, now the picture is clarified. Actually, in addition to the aforementioned reasoning, the pairwise entanglement $C(\rho_{ij})$ follows the probability P_{LHFS} for an arbitrary system size, for either even or odd j. Figure 4 displays that for an even index j, P_{LHFS} decreases with the system size, which is the case for ρ_{12} in Fig. 4(a), and this is why $C(\rho_{ij})$ decreases too with the increase of the system's size L for j even. However, for an odd index j, P_{LHFS} increases instead as L increases, as shown for the pair ρ_{23} in Fig. 4(b) and in this case $C(\rho_{ij})$ increases too with L.

It is appropriate to note that following the reasoning above, the pairwise entanglement of the pair ρ_{14} is greater than ρ_{13}, which is indeed the situation observed in Fig. 1. At first glance, this seems nonobvious and contradicts the distance effect on pairwise entanglement since it is commonly believed that this later decays rapidly as the distance separating the particles grows, in most systems with short-range interaction. However, an easier explanation for this peculiar behavior

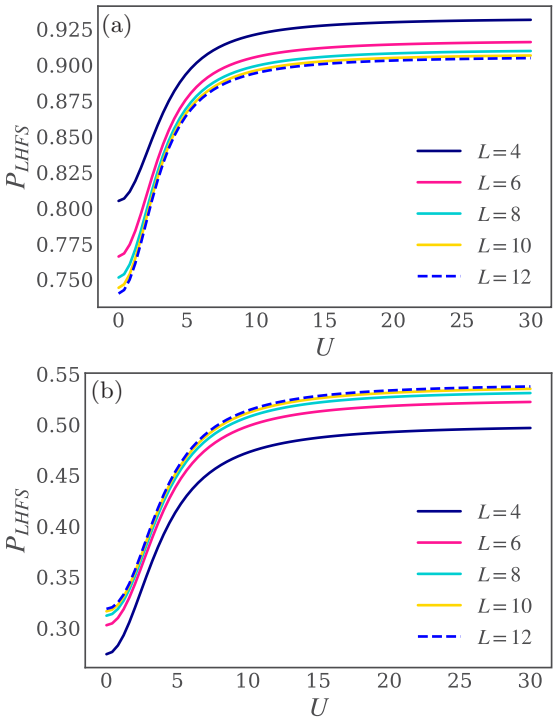

FIG. 4. Probability P_k associated with the LHFS as a function of U with various system sizes L for (a) ρ_{12} and (b) ρ_{23}.

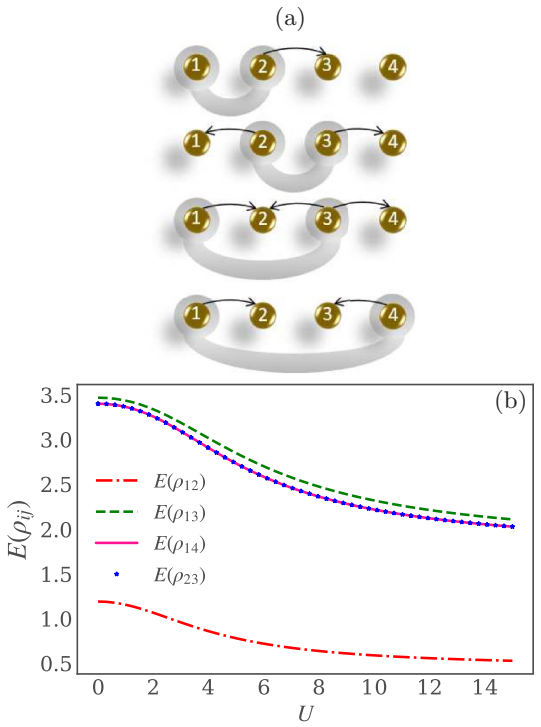

FIG. 5. (a) Representative scheme showing the direct correlation bonds between each pair and the remaining sites for $L = 4$. (b) Entanglement $E(\rho_{ij})$ externally shared by the different pairs for $L = 4$.

can be derived in terms of the entanglement monogamy and Coffman-Kundu-Wootters inequalities [34] through the entanglement that is externally shared by a given pair. We will refer to this type of entanglement as shared entanglement hereafter, which will be quantified using the von Neumann entropy $E(\rho_{ij}) = -\mathrm{Tr}(\rho_{ij}\log_2\rho_{ij})$, where ρ_{ij} is the state describing a pair of quantum dots.

In Fig. 5(a) it is shown that ρ_{14} is directly linked with sites 2 and 3, making two bonds of direct interactions exactly similar to the pair ρ_{23}. This is the reason why they externally share the same amount of entanglement as shown in Fig. 5(b). Furthermore, since they have equal occupation probabilities P_k at $U = 0$ [Fig. 3(a)], $\rho_{23} = \rho_{14}$, which implies that $C(\rho_{23}) = C(\rho_{14})$ at $U = 0$. This is indeed observed in Figs. 1(b) and 1(d) for $L = 4$. In contrast, the pair ρ_{13} makes three direct interaction bonds with sites 2 and 4 [Fig. 5(b)]. For this reason the pair ρ_{13} has to externally share the greatest amount of entanglement $E(\rho_{13})$ compared to all the other pairs, as displayed in Fig. 5(b). Hence, according to the monogamy of entanglement, the pair ρ_{13} is less entangled in comparison to ρ_{14}, thus establishing a long-distance entanglement by the pair ρ_{14} against ρ_{13}.

The local entanglement $E(\rho_i)$ (Fig. 2) and the entanglement $E(\rho_{ij})$ shared by the pairs [Fig. 5(b)] have a maximal value at $U = 0$ because of the rich structure of quantum correlations present in the system. Once U increases, the entanglement decreases and here the quantum correlations are no longer powerful. Nonetheless, the pairwise entanglement $C(\rho_{ij})$ could achieve a maximal value at $U \neq 0$. This quantum picture will be clarified and studied in details in the next section, where a rigorous explanation of the behavior of pairwise entanglement as a function of U will be presented.

C. Pairwise entanglement in the finite coupling regime

Generally, increasing U allows the pairs to favor more the LHFS, except for the pair ρ_{13}, which has a strong tendency to be in a state with $N = 2$ but $S = \{-1, 0, +1\}$ as a mixture that combines the ferromagnetic and the antiferromagnetic behavior associated with this subsystem. It is defined as $\rho = p\sum_{i=1}^{3}|\psi_i\rangle\langle\psi_i|$, with $|\psi_1\rangle = |\uparrow\uparrow\rangle$, $|\psi_2\rangle = |\downarrow\downarrow\rangle$, and $|\psi_3\rangle = \alpha|\uparrow\uparrow\rangle + \beta|\downarrow\downarrow\rangle + \gamma|\uparrow\downarrow\rangle + \delta|\downarrow\uparrow\rangle$. This is clearly shown in Fig. 3, where the probability associated with the LHFS grows faster with U compared to the other states in the mixture characterizing the pairs ρ_{12}, ρ_{23}, and ρ_{14}, whereas for the pair ρ_{13}, it is the probability p associated with $|\psi_1\rangle$, $|\psi_2\rangle$, and $|\psi_3\rangle$ that increases instead and becomes dominant compared to the other probabilities.

Evolving into the favored pure LHFS or the mixed state ρ, while increasing the Coulomb interaction U, each pair ρ_{ij} exhibits an increase of its purity, which is again established from Fig. 3, where the majority of the probabilities P_k vanish. This is among the prominent factors that could increase the pairwise entanglement, as it is widely known that increasing the degree of mixture decreases the entanglement. In our case we observe an increase of the entanglement due to the decrease of the mixture. However, relying solely on this statement is not enough, because as shown in Fig. 1(d) the pairwise entanglement $C(\rho_{14})$ decreases instead; therefore, another factor has to be taken into account. As a matter of fact, the state describing the pairs is given by $\rho_{ij}(U) = \sum_k P(U)|\psi_k(U)\rangle\langle\psi_k(U)|$, in which the states $|\psi_k\rangle$, namely, the LHFSs, evolve also with U at the same time the probabilities P_k evolve. In this regard, we will show that there are two competing effects that are present

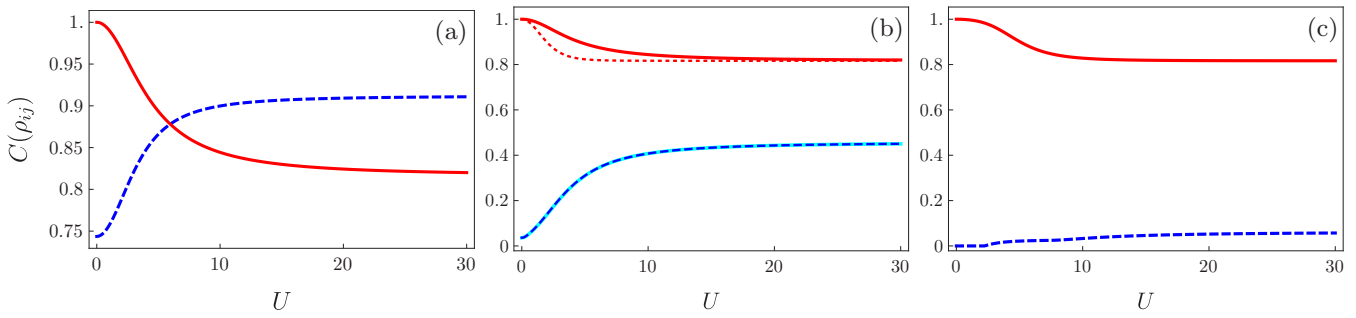

FIG. 6. The LBC associated with the LHFS (red solid and dotted lines) and with the global state ρ_{ij} with a frozen LHFS (blue solid and dashed lines) for (a) ρ_{12}, (b) ρ_{23} and ρ_{14}, and (c) ρ_{13}.

in the system: The mixing effect (the effect of the mixture) and the inherent entanglement effect associated with the dominant LHFS (the effect of the entanglement corresponding to the LHFS).

Based on the previous statement, let us return to the discussion of the pairwise entanglement behavior with the increase of U as plotted in Fig. 1. The two aforementioned effects will play an important role in explaining the behavior of pairwise entanglement, as will be shown in the following.

In order to show the effect of the LHFS entanglement on the global correlations $C(\rho_{ij})$, we have frozen the evolution of the LHFS with U (conserving the state as when $U = 0$) inside the mixture $\sum_k P(U)|\psi_k(U)\rangle\langle\psi_k(U)|$ without freezing the evolution of its associated probability P_{LHFS} such that $\text{Tr}(\rho_{ij}) = 1$ is always satisfied. From Fig. 6 it is clear that with a frozen LHFS, the pairwise entanglement $C(\rho_{ij})$ increases and then stabilizes for large values of U. Apparently, this is due to the decline of the mixing effect shown in Fig. 3, where a majority of the probabilities P_k vanish with U. In contrast, with a nonfrozen LHFS, which is the case in Figs. 1(a)–1(c), the pairwise entanglement $C(\rho_{ij})$ declines when attaining a maximum value, which indicates the considerable effect of the LHFS on pairwise entanglement. In conjunction with that, the entanglement of the LHFS decreases asymptotically, as displayed in Fig. 6. Since the LHFS is the dominant state, its behavior will be dominant, but in the presence of the mixing effect, its behavior appears after a specific value of U, where it is noticeable in Fig. 1 that $C(\rho_{ij})$ decreases asymptotically, In this case, the inherent effect associated with the LHFS dominates the behavior of pairwise correlations.

To be specific, from Fig. 4, for small values of U, the behavior of $C(\rho_{ij})$ is generally controlled by the decline of the mixing effect, resulting in a significant increase of the entanglement in the adjacent sites such as $C(\rho_{12})$ and $C(\rho_{23})$. For the distant sites the increase of entanglement, which appears only in small-size systems since the range of entanglement is limited, starts after an interval of U given the fact that the degree of mixedness in this case is higher and thus the mixing effect persists longer. Beyond that, it is the behavior of the LHFS that becomes the dominant one, where the pairwise entanglement $C(\rho_{ij})$ decreases and follows the entanglement behavior of the LHFS itself. At this stage, with the increase of U, the system is focused on the LHFS with a high probability.

In contrast, for the pair ρ_{14} with $L = 4$ [Fig. 1(d)] the situation is different, where it is clearly shown that the pairwise entanglement $C(\rho_{14})$ decreases instantly with U. The explanation can be further clarified if we look at Fig. 6(b), where the pairs ρ_{23} and ρ_{14} have the same degree of mixture since they have the same probabilities P_k as a function of U [Fig. 3(c)]. Nonetheless, the evolution rate of the LHFS associated with ρ_{14} is considerably faster compared to the LHFS of ρ_{23}. This is expected as long as the correlations at the end sites decay faster as opposed to the middle sites against U (Fig. 2). As a result, the inherent effect associated with the LHFS becomes the dominant one. In this case the behavior of entanglement will be overwhelmed by the behavior of the LHFS itself and here the decline of the mixing effect is no longer able to increase the pairwise entanglement $C(\rho_{ij})$ vs the evolution rate of the LHFS entanglement. Thus the end-to-end pairwise entanglement generally decreases instantly with U, but this behavior is expected to be shown only in small-size systems such as $L = 2$ and 4, since the long-distance entanglement is limited in large-size systems.

V. CONFINEMENT STATE AND GENUINE FOUR-PARTITE ENTANGLEMENT

The Fermi-Hubbard model can accurately describe quantum dots when U tends to infinity. Actually, when the repulsion interaction U within the sites is strong enough, it allows the electrons to move away from each other (thus excluding the sites with double occupancy) and the tunneling of these electrons between the sites is blocked. The situation is similar to the creation of potential barriers between the sites which prohibits the electrons to move outside. This process displays exactly the quantum confinement effect in the Fermi-Hubbard sites and as such the state describing the system is called the confinement state with $N = \frac{L}{2}$ and $S = 0$.

Apparently, systems with different sizes do behave similarly in most cases. In this respect, the stabilization of pairwise entanglement in the confinement state under the variation of U is a common property characterizing the various system sizes. So following the steps in the preceding section, the study of the confinement state will be restricted to the smallest-size system $L = 4$; then some insights can be drawn for larger sizes.

For a small-size array of four quantum dots, the confinement state (in the strong-coupling regime) is given by

$$|\psi_C\rangle = -\alpha(|\downarrow\downarrow\uparrow\uparrow\rangle + |\uparrow\uparrow\downarrow\downarrow\rangle) + \beta(|\downarrow\uparrow\downarrow\uparrow\rangle + |\uparrow\downarrow\uparrow\downarrow\rangle) - \gamma(|\downarrow\uparrow\uparrow\downarrow\rangle + |\uparrow\downarrow\downarrow\uparrow\rangle), \quad (9)$$

where $\alpha = \frac{1}{\sqrt{6}} \approx 0.41$, $\beta = \frac{3\sqrt{8639}}{500} \approx 0.56$, and $\gamma = \frac{\sqrt{16747/3}}{500} \approx 0.15$. When U takes strong values the pairwise entanglement associated with the pairs ρ_{13} and ρ_{14} vanishes, but for ρ_{12} the entanglement stabilizes with an important value, as seen in Fig. 1. It turns out that when $U \to +\infty$ the pairwise entanglement $C(\rho_{23})$ vanishes too and becomes equal to $C(\rho_{14})$. As the LBC is actually just an estimation of the minimal value of entanglement, the conclusions that can be drawn from its behavior can be misleading sometimes and as a consequence have to be taken with much care. However, in this case, this behavior can be confirmed by returning to the well-established measures of entanglement for qubits and using them to get the exact amount of the different pairwise entanglements contained in $|\psi_C\rangle$. As a matter of fact, because each dot can be occupied by one electron with spin $\uparrow$ or $\downarrow$, the state (9) can now represent the state of a two-level system. Consequently, the concurrence (for qubits) [35] is an appropriate measure of the amounts of pairwise entanglement and gives in this case the values $C(\rho_{12}) = 0.866$ and $C(\rho_{23}) = C(\rho_{13}) = C(\rho_{14}) = 0$.

Returning to the discussion about the shared entanglement, given the fact that the pair ρ_{12} is still sharing entanglement with the system when $U \to +\infty$ [Fig. 5(b)], this means that other kinds of quantum correlations, beyond pairwise entanglement, are present, namely, the genuine four-partite entanglement. It turns out that the confinement state $|\psi_C\rangle$ belongs to the generic class that represents one classification of the nine families of the four-qubit pure states defined in [36]. It can be generally written in the computational basis as

$$\begin{aligned}|\psi_G\rangle = {} & \frac{z_0 + z_3}{2}(|0000\rangle + |1111\rangle) + \frac{z_0 - z_3}{2}(|0011\rangle \\ & + |1100\rangle) + \frac{z_1 + z_2}{2}(|0101\rangle + |1010\rangle) \\ & + \frac{z_1 - z_2}{2}(|0110\rangle + |1001\rangle), \end{aligned} \tag{10}$$

with $z_0, z_1, z_2, z_3 \in \mathbb{C}$. For the confinement state $|\psi_C\rangle$ in (9), $z_0 = -z_3 = -\alpha$, $z_1 = \beta - \gamma$, and $z_2 = \beta + \gamma$. The four-tangle for such a state can be defined and computed as [37–39] $\tau_{1234}^{(\psi_C)} = |\sum_{i=0}^{3} z_i^2|^2 = |2(\alpha^2 + \beta^2 + \gamma^2)|^2 = 1$ with $i = 0, 1, 2, 3$. So the confinement state is maximally entangled when it comes to the genuine four-partite entanglement.

It is worth noting that the four-qubit Greenberger-Horne-Zeilinger state belongs also to the same generic family with $z_0 = z_3 = 1/\sqrt{2}$ and $z_1 = z_2 = 0$, where we have $\tau_{1234}^{\mathrm{GHZ}} = |2z_0^2|^2 = 1$.

Thus the Hubbard model's confinement state is genuinely multipartite entangled even for larger sizes. An n-partite entangled state is called genuine if and only if the state is not separable with respect to any m partition ($m \leqslant n$) and this is confirmed by the fact that entanglement $E(\rho_{m/n})$ in the Hubbard model has a nonzero value. However, defining the family class in which the confinement state, as an n-qubit state, belongs is still an interesting question to be answered in future works and seems to get complicated as the system size becomes larger $L > 4$.

VI. CONCLUSION

In this work we have examined the pairwise entanglement in quantum dot systems, formally described by the one-dimensional Fermi-Hubbard model. As ququart systems, the lower bound of concurrence is deemed the appropriate choice to investigate the behavior in the weak-coupling regime. Namely, it is demonstrated that a proper optimization of the Coulomb interaction can create entanglement between quantum dots and even more so help it grow considerably. On a related note, it was shown that the range of entanglement extends to the third-neighbor site for a system size of $L = 4$, whereas it could be created and extended to the third-neighbor site by properly adjusting the Coulomb interaction for $L > 4$.

In addition to that, the size effect was studied and it was shown that under the size effect the pairwise entanglement decreases for the pairs ρ_{ij} with j even as the size grows, whereas it increases if j is odd. In this regard, we have presented a rigorous description of the pairs in terms of the local half-filled state for each pair with a fixed number of electrons $N = 2$ and a spin $S = 0$. Acquaintance with this state provides a proper explanation concerning the amount of pairwise entanglement as well as the behavior of this entanglement against the Coulomb interaction and the size effect. Finally, the study of the confinement state in the system demonstrated the existence of the genuine four-partite entanglement with a maximum value achieved for $L = 4$.

Motivated by these results, it would be of interest to study the genuine multipartite entanglement as well as the family class in which the confinement state belongs for larger sizes. Furthermore, it is clear that the Hubbard model provides an adequate entanglement resource for ququart teleportation; however, as the size increases the end-to-end entanglement vanishes, which would allow us to study in future works some mechanisms to circumvent this by producing long-range entanglement in the Fermi-Hubbard model, thus allowing us to reach maximum teleportation fidelity.

ACKNOWLEDGMENTS

S.A. is grateful for financial support from the National Center for Scientific and Technical Research (CNRST) (Grant No. 1UM5R2018). This research was supported through computational resources of HPC-MARWAN provided by CNRST, Rabat, Morocco. The authors acknowledge fruitful discussions with Z. Mzaouali.

[1] A. Einstein, B. Podolsky, and N. Rosen, Can quantum-mechanical description of physical reality be considered complete? Phys. Rev. **47**, 777 (1935).

[2] B. E. Kane, A silicon-based nuclear spin quantum computer, Nature (London) **393**, 133 (1998).

[3] P. Walther, K. J. Resch, T. Rudolph, E. Schenck, H. Weinfurter, V. Vedral, M. Aspelmeyer, and A. Zeilinger, Experimental one-way quantum computing, Nature (London) **434**, 169 (2005).

[4] S. Pirandola, J. Eisert, C. Weedbrook, A. Furusawa, and S. L.

Braunstein, Advances in quantum teleportation, Nat. Photon. **9**, 641 (2015).

[5] L. Amico, R. Fazio, A. Osterloh, and V. Vedral, Entanglement in many-body systems, Rev. Mod. Phys. **80**, 517 (2008).

[6] F. A. Zwanenburg, A. S. Dzurak, A. Morello, M. Y. Simmons, L. C. L. Hollenberg, G. Klimeck, S. Rogge, S. N. Coppersmith, and M. A. Eriksson, Silicon quantum electronics, Rev. Mod. Phys. **85**, 961 (2013).

[7] D. Loss and D. P. DiVincenzo, Quantum computation with quantum dots, Phys. Rev. A **57**, 120 (1998).

[8] *Quantum Dots for Quantum Information Technologies*, edited by P. Michler (Springer, Cham, 2017).

[9] T. Hensgens, T. Fujita, L. Janssen, X. Li, C. J. Van Diepen, C. Reichl, W. Wegscheider, S. Das Sarma, and L. M. K. Vandersypen, Quantum simulation of a Fermi-Hubbard model using a semiconductor quantum dot array, Nature (London) **548**, 70 (2017).

[10] S. Yang, X. Wang, and S. Das Sarma, Generic Hubbard model description of semiconductor quantum-dot spin qubits, Phys. Rev. B **83**, 161301(R) (2011).

[11] D. Cozzolino, B. Da Lio, D. Bacco, and L. K. OxenlÃ¸we, High-dimensional quantum communication: Benefits, progress, and future challenges, Adv. Quantum Technol. **2**, 1900038 (2019).

[12] Y.-C. Ou, H. Fan, and S.-M. Fei, Proper monogamy inequality for arbitrary pure quantum states, Phys. Rev. A **78**, 012311 (2008).

[13] D. Larsson and H. Johannesson, Single-site entanglement of fermions at a quantum phase transition, Phys. Rev. A **73**, 042320 (2006).

[14] S.-J. Gu, S.-S. Deng, Y.-Q. Li, and H.-Q. Lin, Entanglement and Quantum Phase Transition in the Extended Hubbard Model, Phys. Rev. Lett. **93**, 086402 (2004).

[15] T. J. Osborne and M. A. Nielsen, Entanglement in a simple quantum phase transition, Phys. Rev. A **66**, 032110 (2002).

[16] B.-Q. Jin and V. E. Korepin, Localizable entanglement in antiferromagnetic spin chains, Phys. Rev. A **69**, 062314 (2004).

[17] L. Campos Venuti, C. Degli Esposti Boschi, and M. Roncaglia, Qubit Teleportation and Transfer across Antiferromagnetic Spin Chains, Phys. Rev. Lett. **99**, 060401 (2007).

[18] S. M. Giampaolo and F. Illuminati, Long-distance entanglement in many-body atomic and optical systems, New J. Phys. **12**, 025019 (2010).

[19] L. Campos Venuti, C. Degli Esposti Boschi, and M. Roncaglia, Long-Distance Entanglement in Spin Systems, Phys. Rev. Lett. **96**, 247206 (2006).

[20] T. Byrnes, N. Y. Kim, K. Kusudo, and Y. Yamamoto, Quantum simulation of Fermi-Hubbard models in semiconductor quantum-dot arrays, Phys. Rev. B **78**, 075320 (2008).

[21] J. Hubbard, Electron correlations in narrow energy bands, Proc. R. Soc. London **276**, 238 (1963).

[22] P. Barthelemy and L. M. K. Vandersypen, Quantum dot systems: A versatile platform for quantum simulations, Ann. Phys. (Berlin) **525**, 808 (2013).

[23] R. Okamoto, H. F. Hofmann, S. Takeuchi, and K. Sasaki, Demonstration of an Optical Quantum Controlled-NOT Gate without Path Interference, Phys. Rev. Lett. **95**, 210506 (2005).

[24] K. Chen, S. Albeverio, and S.-M. Fei, Concurrence of Arbitrary Dimensional Bipartite Quantum States, Phys. Rev. Lett. **95**, 040504 (2005).

[25] H.-P. Breuer, Separability criteria and bounds for entanglement measures, J. Phys. A: Math. Gen. **39**, 11847 (2006).

[26] H.-P. Breuer, Optimal Entanglement Criterion for Mixed Quantum States, Phys. Rev. Lett. **97**, 080501 (2006).

[27] J. I. de Vicente, Lower bounds on concurrence and separability conditions, Phys. Rev. A **75**, 052320 (2007).

[28] M. Li, S.-M. Fei, and Z.-X. Wang, A lower bound of concurrence for multipartite quantum states, J. Phys. A: Math. Theor. **42**, 145303 (2009).

[29] X.-N. Zhu, M. Li, and S.-M. Fei, in *Foundations of Probability and Physics - 6, Växjö, 2011*, edited by M. D'Ariano, S. M. Fei, E. Haven, B. Hiesmayr, G. Jaeger, A. Khrennikov, and J.-Å. Larsson, AIP Conf. Proc. No. **1424** (AIP, Melville, 2012), p. 77.

[30] L. C. Venuti and M. Roncaglia, Analytic Relations between Localizable Entanglement and String Correlations in Spin Systems, Phys. Rev. Lett. **94**, 207207 (2005).

[31] P. Weinberg and M. Bukov, QuSpin: A Python package for dynamics and exact diagonalisation of quantum many body systems part I: Spin chains, SciPost Phys. **2**, 003 (2017).

[32] P. Weinberg and M. Bukov, QuSpin: A Python package for dynamics and exact diagonalisation of quantum many body systems. Part II: Bosons, fermions and higher spins, SciPost Phys. **7**, 020 (2019).

[33] M. C. B. Sousa and C. A. Macedo, Thermodynamic properties of the Hubbard model for a diatomic molecule *AB*, Sci. Plena **4**, 094401 (2011).

[34] V. Coffman, J. Kundu, and W. K. Wootters, Distributed entanglement, Phys. Rev. A **61**, 052306 (2000).

[35] W. K. Wootters, Entanglement of Formation of an Arbitrary State of Two Qubits, Phys. Rev. Lett. **80**, 2245 (1998).

[36] F. Verstraete, J. Dehaene, B. De Moor, and H. Verschelde, Four qubits can be entangled in nine different ways, Phys. Rev. A **65**, 052112 (2002).

[37] S. S. Bullock and G. K. Brennen, Canonical decompositions of *n*-qubit quantum computations and concurrence, J. Math. Phys. **45**, 2447 (2004).

[38] G. Gour, S. Bandyopadhyay, and B. Sanders, Dual monogamy inequality for entanglement, J. Math. Phys. **48**, 012108 (2007).

[39] B. Paul, K. Mukherjee, A. Sen, D. Sarkar, A. Mukherjee, A. Roy, and S. S. Bhattacharya, Persistency of genuine correlations under particle loss, Phys. Rev. A **102**, 022401 (2020).